

Poly(2,5-dimercapto-1,3,4-thiadiazole)/sulfonated graphene composite as cathode material for rechargeable lithium batteries

Lifeng Jin · Gengchao Wang · Xingwei Li ·
Liangbin Li

Received: 5 February 2010/Accepted: 10 November 2010/Published online: 24 November 2010
© Springer Science+Business Media B.V. 2010

Abstract Poly(2,5-dimercapto-1,3,4-thiadiazole) (PDMcT)/sulfonated graphene conductive composite (PDMcT/SGS) was synthesized through in situ oxidative polymerization in the presence of the water-soluble sulfonated graphene sheets (SGS). Raman spectra revealed the existence of the $\pi-\pi$ interaction between thiadiazole rings and basal planes of SGS. Scanning electron microscopy and transmission electron microscopy showed that the submicron-sized petals and nanofibers of PDMcT grew onto the surface of SGS. As evidenced by the cyclic voltammetry results, the incorporation of SGS has significantly improved the electrochemical activity and cyclability of PDMcT. The discharge capacity of PDMcT/SGS composite, measured with the charge-discharge tests, was 268 mAh g⁻¹ at the first cycle and 124 mAh g⁻¹ after 10 cycles.

Keywords Poly(2,5-dimercapto-1,3,4-thiadiazole) · Graphene · In situ polymerization · Rechargeable lithium batteries · Cathode material

1 Introduction

During the past 20 years, the organodisulfide compounds have attracted considerable attention because of their potential use as the organic/polymeric cathode materials

with high energy density, lightweight, and environmental friendliness in lithium batteries [1–8]. Among those organodisulfide compounds, 2,5-dimercapto-1,3,4-thiadiazole (DMcT) is one of the most promising materials since it possesses high theoretical specific capacity and high stability to temperature [9, 10]. However, the application of the DMcT has been hindered due to its poor electrically conductivity and low redox rate at room temperature [11].

In order to overcome these hurdles, many materials, such as conductive polymers [2, 12–16], metal nanoparticles (Ag, Pd) [17–19], carbon fibers [20] and so on have been used as electrocatalysts, to accelerate the redox reactions of DMcT and provide a sufficient conductive pathway. However, these composite cathode materials do not have sufficient charge/discharge cyclability for practical application.

Graphene, a flat monolayer of hexagonally arrayed sp²-bonded carbon atoms, has recently attracted considerable attention for its potential applications in many technological fields [21–29]. Graphene as nanometer-sized filler can form conductive pathways in the composites even at an extremely small concentration because of its high electrical conductivity and a large surface-to-volume ratio [23]. A variety of graphene composites based on various polymers such as polystyrene [23], polyaniline [24], polystyrenesulfonate-doped poly(3,4-ethylenedioxythiophene) [25], epoxy [28], polyurethane [30], poly(vinylidene fluoride) [31], and poly(arylene sulfide) [32] have been reported.

However, graphene nanosheets form irreversible coagulation in water due to their hydrophobic characteristic, which restricts homogeneous dispersion of the graphene nanosheets in polymer matrices at the individual sheet level. Therefore, the preparation of water-soluble graphene sheets is crucial. Water-soluble graphene sheets are usually

L. Jin · G. Wang (✉) · X. Li · L. Li
Shanghai Key Laboratory of Advanced Polymeric Materials,
Key Laboratory for Ultrafine Materials of Ministry of Education,
School of Materials Science and Engineering, East China
University of Science and Technology, Shanghai 200237,
People's Republic of China
e-mail: gengchaow@ecust.edu.cn

prepared by chemical modifications [33, 34] or non-cova-lent functionalizations [35, 36].

In this article, we will report the synthesis of water-soluble sulfonated graphene sheets (SGS) and the following synthesis of poly(2,5-dimercapto-1,3,4-thiadiazole) (PDMcT)/SGS composite using *in situ* oxidative polymerization method for the first time. The PDMcT/SGS composite obtained has high electrical conductivity and good electrochemical properties compared with pure PDMcT.

2 Experimental

2.1 Materials

DMcT (Acros) was purified through recrystallization from ethanol. Graphite oxide (GO) was synthesized from natural graphite powder (30–50 μm) using the Hummers method [37]. All other reagents were received as analytical grade and were used without further purification.

2.2 Preparation of SGS

The SGS were synthesized using the method reported in the literature [33] and described below. 1-g GO was dispersed in 200 mL deionized water whose pH was adjusted to 9–10 with a NaOH solution. The GO sheets formed after a 2 h sonification. The mixture was then reduced with 3-g sodium borohydride at 80 °C for 1 h under constant stirring. After being centrifuged and rinsed with deionized water, the partially reduced GO was re-dispersed in 100-g deionized water by mild sonification. The above sample was sulfonated with 1.3-g aryl diazonium salt of sulfanilic acid in an ice bath for 3 h. The post-reduction with 15-g hydrazine was carried out at 100 °C for 24 h to remove the remaining oxygen functional groups. The S content of the SGS obtained from elemental analysis is 1.35%.

2.3 Synthesis of PDMcT

1.5 g (10 mmol) of DMcT was dissolved in 100 mL of mixed solvent of deionized water and ethanol (deionized water/ethanol = 1/2, by volume). Then 2.54 g (10 mmol) of iodine (dissolved in 40 mL of ethanol) was dropped into the above solution. The polymerization continued for 24 h at 40 °C with a continuous stirring. The reaction mixture was filtered, and then washed with ethanol until the filtrate was colorless. The product obtained was dried at 70 °C for 24 h.

2.4 Synthesis of PDMcT/SGS composite

1.5 g (10 mmol) of DMcT was dissolved in 100 mL of mixed solvent of deionized water and ethanol (deionized

water/ethanol = 1/2, by volume), and then 1.5 g of SGS was added into the above solution. The resulting mixture was sonified for 15 min. 2.54 g (10 mmol) of iodine (dissolved in 40 mL of ethanol) was dropped into the above mixture. The reaction was carried out under stirring for 24 h at 40 °C. The resulting product was filtered, washed with ethanol solution, and dried at 70 °C for 24 h, leading the PDMcT/SGS composite. The S content of the PDMcT/SGS composite obtained from elemental analysis is 26.7%. Thus, the PDMcT content in composite was calculated to be 40.5 wt% according as the value of S content of the SGS and the composite.

2.5 Measurements

Fourier-transform infrared spectroscopy (FTIR) spectra were obtained through a Nicolet 5700 spectrometer using KBr sample pallets. Renishaw in Via + Reflex using a 50 mW He–Ne laser was utilized to generate Raman spectra at 785 nm wavelength. A Rigaku D/Max 2550 VB/PC X-ray diffractometer using the Cu K α radiation served as the instrument in the study of X-ray diffraction (XRD) patterns, which were recorded from 3° to 50° (2 θ -angle). The morphology of the samples was observed using both scanning electron microscopy (SEM, JEOL JSM-6360) and transmission electron microscopy (TEM, JEOL JEM-2100 at the accelerating voltage of 200 kV). A TGA/SDTA/851e thermogravimetric analyzer, which was used to perform thermogravimetric analysis (TGA), recorded the weight loss of the samples that were heated from room temperature to 800 °C at 10 °C min $^{-1}$ under nitrogen. The electrical conductivity of the samples was determined using a SX 1934 four-probe instrument with four-probe method on compressed pellets.

Cyclic voltammetry experiments were performed using a CHI 760C electrochemical analyzer with a standard three-electrode system. A platinum foil coated with active materials (PDMcT or PDMcT/SGS composite) was used as working electrode, Ag/AgCl (sat. KCl) electrode was used as the reference electrode and a platinum wire was used as the counter electrode. The charge–discharge tests were carried out on LAND CT2001A using a constant current density of 10 mA g $^{-1}$ and a charge–discharge potential ranging between 1.8 and 4.0 V (vs. Li/Li $^{+}$). The lithium batteries were assembled with a lithium anode, a 1 M LiPF $_6$ /EC-DMC (1:1 by volume) electrolyte, and a cathode made of the composite containing the materials (70 wt% PDMcT + 20 wt% graphite powder, or 90 wt% PDMcT/SGS composite) and an binder (10 wt%). All electrochemical experiments were completed at room temperature under an inert atmosphere.

3 Results and discussion

The FTIR spectra of SGS, PDMcT, and PDMcT/SGS composite are given in Fig. 1. The spectrum of the SGS (Fig. 1a) illustrates the presence of C=C ($\nu_{C=C}$ at $1,565\text{ cm}^{-1}$) and $-SO_3H$ ($\nu_{O=S=O}$ at $1,033$ and $1,003\text{ cm}^{-1}$). The absorption bands of the PDMcT (Fig. 1c) appearing at $1,381$ and $1,047\text{ cm}^{-1}$ correspond to the characteristic absorption of S–S and C–S, respectively. For the PDMcT/SGS composite (Fig. 1b), its spectrum contains the absorption bands of both the PDMcT ($1,381$ and $1,047\text{ cm}^{-1}$) and the SGS ($1,567\text{ cm}^{-1}$).

Figure 2 shows Raman spectra of SGS, PDMcT, and PDMcT/SGS composite. The Raman spectrum of SGS displays a broad G band at $1,603\text{ cm}^{-1}$ and a broad D band at $1,355\text{ cm}^{-1}$ (Fig. 2a). Compared with the graphene reported by Stankovich et al. [38], the G band of SGS is found broadened and red-shifted by 20 cm^{-1} , which might be attributed to a decrease in the average size of the in-plane sp^2 domains due to diazotization and reduction in two stages. For pure PDMcT (Fig. 2c), the characteristic bands showing at 1380 , 1084 , 643 , and 520 cm^{-1} can be assigned to the C=N stretch, the N–N stretch, the symmetric C–S–C stretch, and the S–S stretch, respectively. The Raman spectrum of PDMcT/SGS composite contains the characteristic bands of both SGS ($1,608$ and $1,358\text{ cm}^{-1}$) and PDMcT (1380 , 1074 , 637 , and 520 cm^{-1}) (Fig. 2b). However, comparing with pure PDMcT, one can find that the N–N stretch and the symmetric C–S–C stretch of the thiadiazole rings in PDMcT/SGS composite shifts to lower wavenumbers. This might be due to the π – π interaction between the thiadiazole rings and the basal planes of SGS.

The SEM and TEM pictures of SGS and PDMcT/SGS composite are presented in Fig. 3. The SEM micrograph of SGS (Fig. 3a) shows a number of isolated single- or multi-

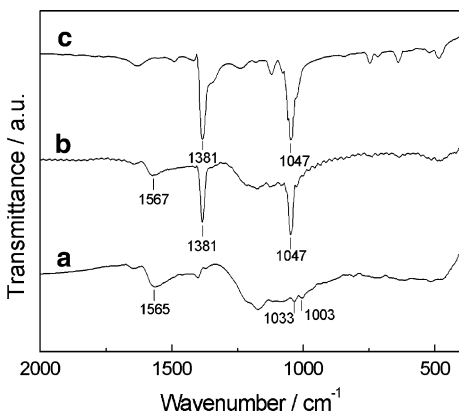


Fig. 1 FTIR spectra of (a) SGS, (b) PDMcT/SGS composite, and (c) PDMcT

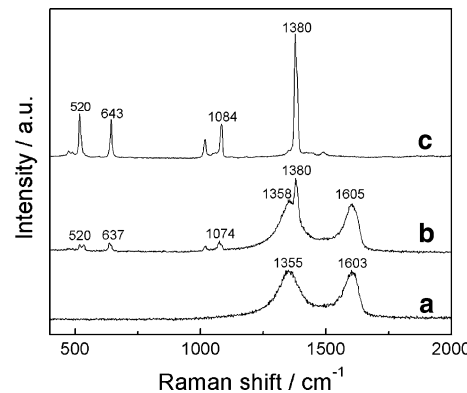


Fig. 2 Raman spectra of (a) SGS, (b) PDMcT/SGS composite, and (c) PDMcT

layer lamellae. From TEM image of SGS (Fig. 3b), one can find the SGS are transparent, crumpled, and folded. However, the PDMcT/SGS composite has a different morphology comparing with SGS. As shown in Fig. 3c, the PDMcT grows onto the surface of SGS and forms submicron-sized petals (indicated as domain 1) and nanofibers (indicated as domain 2). From TEM image of this composite (Fig. 3d), one can also observe that the fiber-like PDMcT with a diameter of 10 – 30 nm deposits onto the surface of SGS nanosheets, indicating that the π – π interaction between PDMcT and SGS plays a pivotal role in the formation of ordered PDMcT chains.

Figure 4 depicts the XRD patterns of SGS, PDMcT, and PDMcT/SGS composite. The XRD pattern of SGS (Fig. 4a) has a broad peak at around $2\theta = 25.2^\circ$. The peak corresponds to the diffraction of the (002) plane composed of sulfonated graphene. The PDMcT exhibits several strong reflection peaks at $2\theta = 20.7^\circ$, 26.3° , 27.8° , and 31.9° , indicating that the PDMcT has better crystalline structure (Fig. 4c). In the diffractogram of PDMcT/SGS composite, all diffraction peaks attributing to the PDMcT remain while the peak corresponding to the (002) plane of SGS disappears. This could be explained with the formation of irregular stack of SGS resulted from PDMcT deposition onto the surface of SGS.

TGA curves for SGS, PDMcT, and PDMcT/SGS composite are shown in Fig. 5. The thermogram of pure PDMcT shows a weight loss of 99.7 wt\% in a nitrogen atmosphere at $700\text{ }^\circ\text{C}$ (Fig. 5a). However, the SGS lost only 21 wt\% of its original weight under the same condition (Fig. 5c). The higher thermal stability of SGS than that of GO may result from the removal of the labile oxygen functional groups by chemical reduction [39]. For the PDMcT/SGS composite, the weight loss in a nitrogen atmosphere at $700\text{ }^\circ\text{C}$ is 62.7 wt\% (Fig. 5b), which indicates that the thermal stability of PDMcT is improved with the incorporation of SGS.

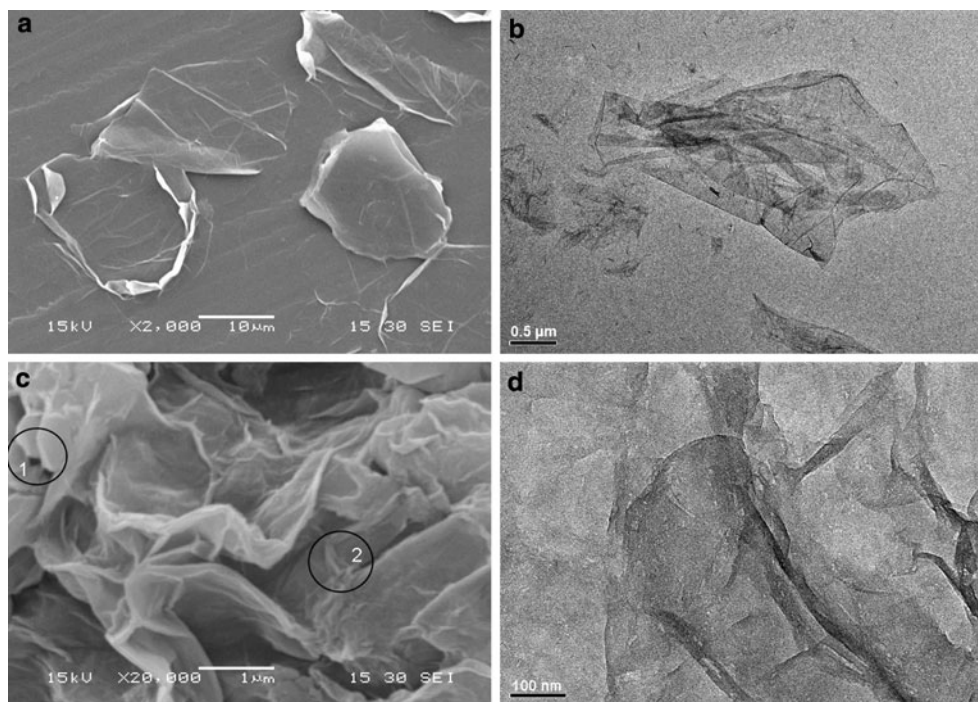


Fig. 3 SEM images of **a** SGS, and **c** PDMcT/SGS composite. TEM images of **b** SGS, and **d** PDMcT/SGS composite

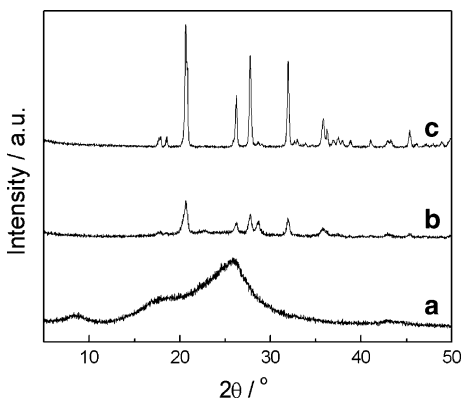


Fig. 4 XRD patterns of **(a)** SGS, **(b)** PDMcT/SGS composite, and **(c)** PDMcT

The electrical conductivity values of PDMcT, SGS, and PDMcT/SGS composite are listed in Table 1. The electrical conductivity of PDMcT is very low ($<1 \times 10^{-7} \text{ S cm}^{-1}$), showing an insulating property while the conductivity of SGS is quite high (2.5 S cm^{-1}). The PDMcT/SGS composite reaches a conductivity value of 0.84 S cm^{-1} , which is approaching that of the pure SGS and over 6 orders of magnitude larger than that of pure PDMcT. The enhanced conductivity of PDMcT/SGS is because the incorporation of SGS that has a large surface-to-volume ratio and good dispersibility, which favors the formation of the conductive pathway.

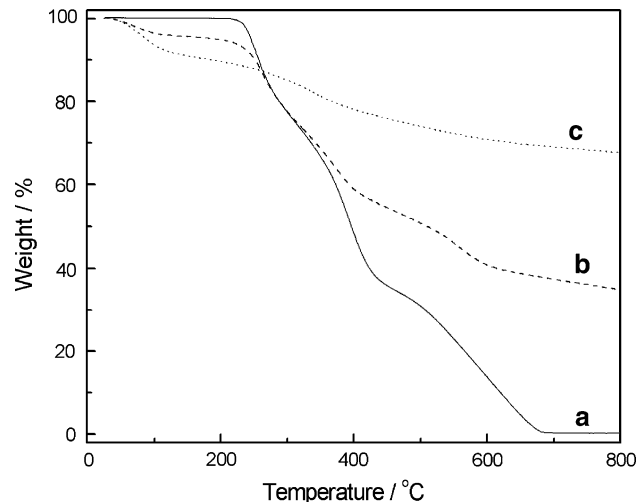


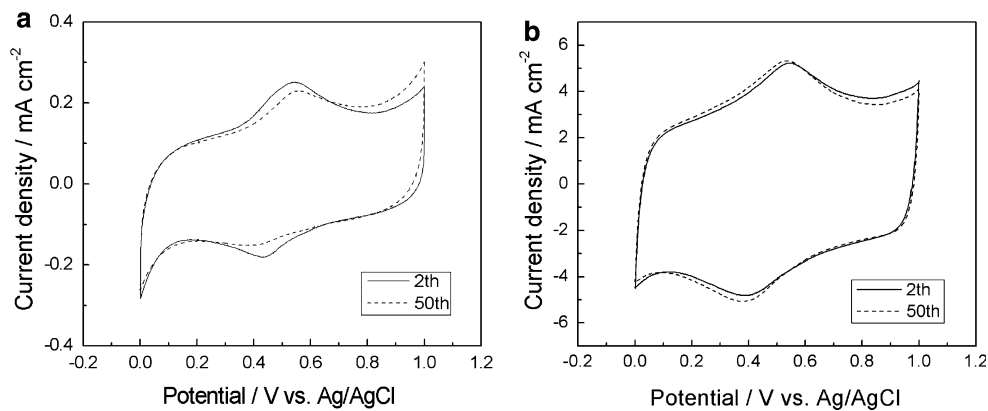
Fig. 5 TGA curves of **(a)** PDMcT, **(b)** PDMcT/SGS composite, and **(c)** SGS

Table 1 Electrical conductivity of PDMcT, SGS, and PDMcT/SGS composite

	PDMcT	SGS	PDMcT/SGS composite
Conductivity (S cm^{-1})	$<1 \times 10^{-7}$	2.5	0.84

Figure 6a, b depict the second and fiftieth cyclic voltammograms of the pure PDMcT and PDMcT/SGS composite, respectively. It can be seen that the all

Fig. 6 The second and fiftieth cyclic voltammogram curves of **a** PDMcT and **b** PDMcT/SGS composite in 1 M LiPF₆/EC-DMC (1:1 by volume) solution at a scanning rate of 20 mV s⁻¹



samples exhibit one pair of redox peaks. The cathodic peak located between 0.39 and 0.43 V is attributed to the depolymerization of PDMcT, while the corresponding anodic peak staying at 0.54–0.56 V is assigned to the polymerization of DMcT. The values of redox current peaks of PDMcT/SGS composite are about 20 times higher than those of pure PDMcT, which indicates that the rate of redox reaction of PDMcT is accelerated remarkably when PDMcT is modified by SGS. This is because the incorporation of SGS of high electrical conductivity and a large surface-to-volume ratio improves electron transport in PDMcT phase.

It can also be found that the current response of pure PDMcT decreases and a reduction peak almost disappears at 50th cycles (Fig. 6a). This is because the DMcT and oligo-DMcT molecules which are produced during the reduction process can gradually dissolve in the organic electrolyte solution [6, 40]. However, the PDMcT/SGS composite displays extraordinary stabilization during the electrochemical cycles (Fig. 6b). The excellent cyclability of PDMcT/SGS composite could be explained as follows. Since SGS possesses large surface area and contains –SO₃H groups, a number of reductive products (DMcT and oligo-DMcT) can be adsorbed on the surface of SGS through the π–π interaction, which inhibits dissolution of the reductive products in the organic electrolyte.

The first charge–discharge curves for lithium batteries with PDMcT and PDMcT/SGS composite as cathode materials are given in Fig. 7. It is noted that both Li-PDMcT battery and Li-PDMcT/SGS battery have one evident discharging platform near 2.4 V, which might be ascribed to the reduction process of the S–S bonds. It is also seen from Fig. 7 that the discharge capacity of Li-PDMcT/SGS battery (268 mAh g⁻¹) is higher than that of Li-PDMcT battery (256 mAh g⁻¹). The improved discharge capacity might be due to the unique structure of PDMcT/SGS composite. The nanometer-sized PDMcT deposits on the surface of SGS uniformly, which reduces the diffusion distance of ions in PDMcT phase during

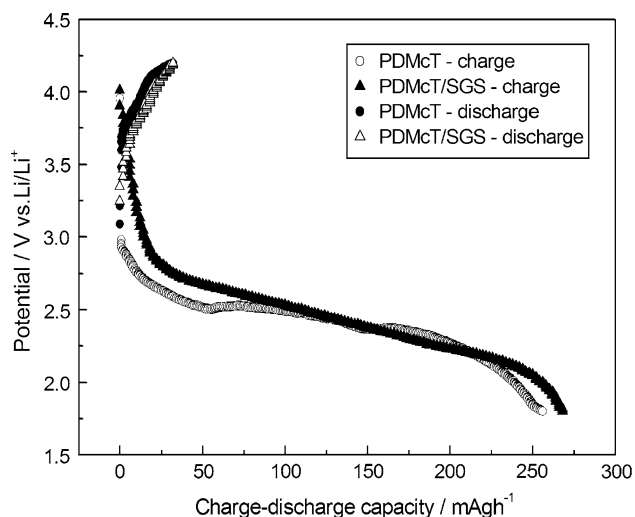


Fig. 7 The first charge–discharge curves for Li-PDMcT battery and Li-PDMcT/SGS battery. Current density: 10 mA g⁻¹. Cutoff voltages: 1.8–4.0 V

charge–discharge process, ensures a high utilization of PDMcT, and then exhibits a high specific capacity.

Figure 8 shows the charge–discharge cycles of Li-PDMcT battery and Li-PDMcT/SGS battery. It can be found from Fig. 8a that the cycle life of Li-PDMcT battery is very short. The discharge capacity decreased substantially to 54 mAh g⁻¹ after second cycle and remained at only 12 mAh g⁻¹ after 6 cycles. As shown in Fig. 8b, when PDMcT/SGS composite is used as the material, the cycle behavior is significantly improved, which is in good agreement with the cyclic voltammogram result. The discharge capacity of the PDMcT/SGS composite can remain at 124 mAh g⁻¹ after 10 cycles. The enhancement of the cycle stability for PDMcT/SGS composite could be related to that the reductive products (DMcT and oligo-DMcT) are adsorbed on the surface of SGS firmly due to the π–π interaction, decreasing dissolution of the reductive products in liquid electrolyte solution.

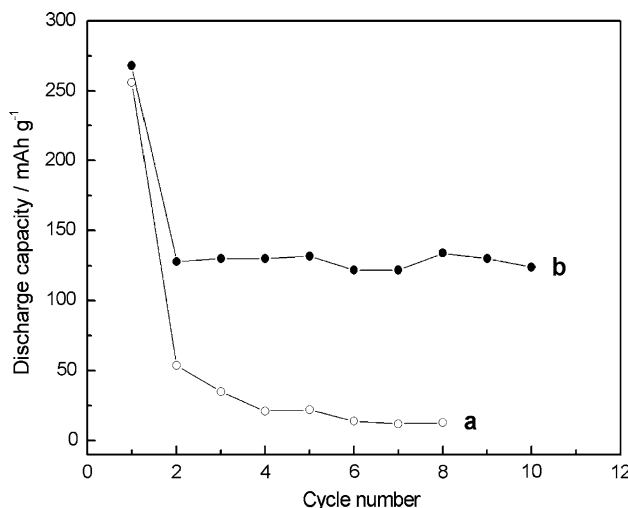


Fig. 8 Variation of discharge capacity for (a) Li-PDMcT battery and (b) Li-PDMcT/SGS battery with cycle number. Current density: 10 mA g^{-1} . Cutoff voltages: 1.8–4.0 V

4 Conclusions

A novel PDMcT/SGS conductive composite was successfully synthesized using in situ oxidative polymerization in mixed solvent of water and ethanol. The electrical conductivity of PDMcT/SGS composite was remarkably improved with the incorporation of SGS because the SGS has a large surface-to-volume ratio and good dispersibility. The enhanced redox properties and improved electrochemical stability are confirmed by the cyclic voltammetry and the charge–discharge tests. The PDMcT/SGS composite may be a promising cathode material for rechargeable lithium batteries.

Acknowledgments We greatly appreciate the financial supports of National Natural Science Foundation of China (50773020, 21044005), Innovation Program of Shanghai Municipal Education Commission (11ZZ55), Shanghai Municipal Science and Technology Commission (0852nm02000), Shanghai Leading Academic Discipline Project (B502) and Shanghai Key Laboratory Project (08DZ2230500).

References

- Visco SJ, De Jonghe LC (1988) J Electrochem Soc 135:2905
- Oyama N, Tatsuma T, Sato T, Sotomura T (1995) Nature 373:598
- Tsutsumi H, Oyari Y, Onimura K, Oishi T (2001) J Power Sources 92:228
- Wang J, Yang J, Xie J, Xu N (2002) Adv Mater 14:963
- Xue L, Li J, Hu S, Zhang M, Zhou Y, Zhan C (2003) Electrochim Commun 5:903
- Deng S, Kong L, Hu G, Wu T, Li D, Zhou Y, Li Z (2006) Electrochim Acta 51:2589
- Amaike M, Iihama T (2006) Synth Met 156:239
- Su Y, Dong W, Zhang J, Song J, Zhang Y, Gong K (2007) Polymer 48:165
- Visco SJ, Mailhe CC, De Jonghe LC, Armand MB (1989) J Electrochem Soc 136:661
- Naoi K, Kawase K, Inoue Y (1997) J Electrochim Soc 144:L173
- Liu M, Visco SJ, De Jonghe LC (1990) J Electrochim Soc 137:750
- Naoi K, Menda M, Ooike H, Oyama N (1991) J Electroanal Chem 318:395
- Yu L, Wang X, Li J, Jing X, Wang F (1998) J Power Sources 73:261
- Li J, Zhan H, Zhou Y (2003) Electrochim Commun 5:555
- Shu D, Zhang J, He C, Meng Y, Chen H, Zhang Y, Zheng M (2006) J Appl Electrochim 36:1427
- Kiya Y, Iwata A, Sarukawa T, Henderson JC, Abruna HD (2007) J Power Sources 173:522
- Park JE, Park SG, Koukitu A (2003) J Electrochim Soc 150:A959
- Park JE, Hatozaki O, Oyama N (2003) Chem Lett 32:138
- Park JE, Park SG, Koukitu A (2004) Synth Met 140:121
- Canobre SC, Davoglio RA, Biaggio SR, Rocha-Filho RC, Bocchi N (2006) J Power Sources 154:281
- Novoselov KS, Geim AK, Morozov SV, Jiang D, Zhang Y, Dubonos SV, Grigorieva IV, Firsov AA (2004) Science 306:666
- Geim AK, Novoselov KS (2007) Nat Mater 6:183
- Stankovich S, Dikin DA, Domke GHB, Kohlhaas KM, Zimney EJ, Stach EA, Piner RD, Nguyen ST, Ruoff RS (2006) Nature 442:282
- Wang D, Li F, Zhao J, Ren W, Chen Z, Tan J, Wu ZS, Gentle I, Lu G, Cheng H (2009) ACS Nano 3:1745
- Hong W, Xu Y, Lu G, Li C, Shi G (2008) Electrochim Commun 10:1555
- Watcharotone S, Dikin DA, Stankovich S, Piner R, Jung I, Domke GHB, Evmeneko G, Wu S, Chen S, Liu C, Nguyen ST, Ruoff RS (2007) Nano Lett 7:1888
- Wang X, Zhi L, Tsao N, Tomovic Z, Li J, Mullen K (2008) Angew Chem Int Ed 47:2990
- Liang J, Wang Y, Huang Y, Ma Y, Liu Z, Cai F, Zhang C, Gao H, Chen Y (2009) Carbon 47:922
- Park N, Hong S, Kim G, Jhi SH (2007) J Am Chem Soc 129:8999
- Raghu AV, Lee YR, Jeong HM, Shin CM (2008) Macromol Chem Phys 209:2487
- Ansari S, Giannelis EP (2009) J Polym Sci Part B 47:888
- Du X, Yu Z, Dasari A, Jun M, Mo M, Meng Y, Mai Y (2008) Chem Mater 20:2066
- Si Y, Samulski ET (2008) Nano Lett 6:1679
- Li D, Muller MB, Gilje S, Kaner RB, Wallace GG (2008) Nat Nanotechnol 3:101
- Stankovich S, Piner RD, Chen XQ, Wu NQ, Nguyen ST, Ruoff RS (2006) J Mater Chem 16:155
- Bai H, Xu Y, Zhao L, Li C, Shi G (2009) Chem Commun 1667
- Hummers WS, Offeman RE (1958) J Am Chem Soc 80:1339
- Stankovich S, Dikin DA, Piner RD, Kohlhaas KA, Kleinhammes A, Jia Y, Wu Y, Nguyen ST, Ruoff RS (2007) Carbon 45:1558
- Shen J, Hu Y, Li C, Qin C, Ye M (2009) Small 5:82
- Doeff MM, Visco SJ, De Jonghe LC (1992) J Electrochim Soc 139:1808